RSC Advances

ROYAL SOCIETY OF CHEMISTRY

www.rsc.org/advances

Journal Name

ARTICLE

Metal-Organic Green Dye: Chemical and Physical Insight Into a Modified Zn-Benzoporphyrin for Dye-Sensitized Solar Cells.

Received 00th January 20xx,
Accepted 00th January 20xx

DOI: 10.1039/x0xx00000x

www.rsc.org/

Gloria Zanotti[a], Nicola Angelini[a], Giuseppe Mattioli[a], Anna Maria Paoletti[a], Giovanna Pennesi[a], Gentilina Rossi[a], Daniela Caschera[b], Luisa De Marco[c], Giuseppe Gigli[d,e]

A new green unsymmetrical zinc triphenyl-tetrabenzoporphyrin compound, i.e. 5,10,15-(triphenyl),20-[ethynyl-(4-carboxy)phenyl]tetrabenzoporphyrinate Zn(II), has been synthesized as the first of a new class of dyes suitable for Dye-Sensitized Solar Cells. The molecule shows a hybrid porphyrin-phthalocyanine structure that allows a finer chemical and physical properties tuning with respect to phthalocyanines, by means of substitutions at the meso-positions, and a UV-Vis spectrum that shows both an intense Soret band at 456 nm and a detectable Q band at 655 nm. The photophysical and redox properties of the molecule have been studied and show that HOMO and LUMO energy values are properly positioned for an effective charge transfer. DFT-based ab initio calculations have confirmed the energetic position of frontier orbitals and highlight the intricate structure of the visible spectrum and the charge transfer behavior of the molecule seen as a part of a complex device. Finally, dye-sensitized solar cells have been realized, IPCE and photovoltaic parameters have been measured, showing preliminary efficiency values of about 2%.

Introduction

In the last twenty years, Dye-Sensitized Solar Cells (DSSCs)have attracted the attention of many researchers because they are an appealing low cost favorable solution to the problem of electrical power supply. They are potentially less expensive, compared to silicon-based solid-state devices, and offer the possibility to provide semitransparent and flexible devices very useful in architectural applications[1].

DSSCs exploit the intense absorption of light of photosensitive molecules like dyes. In such multicomponent devices the role of sensitive dyes is still crucial and the optimization of their chemical structures and properties is considered as extremely important in order to maximize theirs chemical stability, light-harvesting and electronic properties. Different dye families have been tested and studied in the last two decades and, even if in the last few years new materials such as perovskites have shown to be exceedingly promising in this field, a huge amount of work is still in progress to synthesize new dyes with improved performancesand employ the corresponding devices for Building Integrated Photovoltaics (BIPVs) applications.

Until 2011, the most significant results in this field have been achieved by using Ru-based compounds which have given the best conversion efficiency of 11.4%[2,3]. However, due to a number of drawbacks regarding the low natural abundance of ruthenium, the low optical absorbance in the red/near infrared regions and the low molar extinction coefficient of the Ru compounds, other dye families have been intensively investigated. Among the most studied compounds there are metallo-porphyrins and -phthalocyanines, also inspired by natural photosynthetic processes. The strong and widely tunable absorption properties of their extended π-conjugated macrocycles make them particularly versatile in different architectures of solar cells.[4,5]In particular the integration of solar panels in windows and buildings encounters the problem of lacking of stable blue and green dyes. In this sense it appears extremely important to find outand investigate the photovoltaic properties of dyesof such colors.

A long synthetic job is required to build up molecules of such kind which possess all the requirements to be implemented in a DSSC. In particular synthetic strategies oriented towards donor-pi-acceptor (D-π-A) systems, capable of limiting the recombination between photogenerated electrons and holes, have been favored. Porphyrin and phthalocyanine macrocycles have been indeed peripherally substituted by inserting electron-donor groups and the molecules have been generally provided of one or more electron-acceptor anchoring groups for covalent attachment to semiconducting (e.g., TiO_2-based) electrodes. More specifically, many D-π-A porphyrin systems have been synthesized and extensively characterized. In 2010, the YD2 sensitizer, a D-π-A zinc porphyrin, has achieved a record efficiency of 11% for DSSC devices[6]. Further

[a] CNR – ISM Via Salaria km 29.500, Monterotondo Scalo (Rm), 00015-Italy.
[b] CNR - ISMN, Via Salaria km 29.500, Monterotondo Scalo (Rm), 00015-Italy.
[c] IIT - Center for Biomolecular Nanotechnologies, Via Barsanti, Arnesano (Le), 73010 -Italy
[d] CNR-NANOTEC Via Amendola 122/D - Bari 70126-Italy.
[e] Dip. di Matematica e Fisica, Università del Salento, Lecce, 73100, Italy

modifications to its structure have allowed to obtain the YD2-*o*-C8 derivative, which have reached the impressive value of η = 12.6%, further raised to exceed 13% when employed in a cocktail mixture with the metal-free dye Y123 and this is nowadays the best performance in the whole DSSC field[7].

Phthalocyanines have also been widely tested in photovoltaic devices. Their intense absorption in the red/near-IR region of the solar spectrum, their large extinction coefficient and their outstanding thermal and photochemical stability make them good candidates as materials for solar-cell applications[5]. However, despite such promising properties, the efficiency of DSSCs employing phthalocyanines as sensitizers has never been impressive. This is likely due to the fact that they are less soluble than porphyrins, have a strong tendency to aggregate on the TiO_2 surface and are often characterized by an unfavorable energetic position of their frontier orbitals with respect to the electrochemical potentials of the electrolyte and of the TiO_2 conduction band. At any rate, the most efficient devices have been reported by Torres et al., employing peripherally substituted Zn phthalocyanines holding rigid π-conjugated bridges (double and triple C-C bonds) between the anchoring carboxylic groups and the macrocycle, that showed efficiencies up to 6.13%[8], and by Mori, Kimura et al., whose PcS20 is the most efficient phthalocyanine-based dye showing a 6.4% efficiency value[9].

Given the research framework discussed above, we have tried to merge all the interesting properties of porphyrin- and phthalocyanine-based dyes by focusing on a class of compounds having average properties between such molecular architectures, namely, the tetrabenzoporphyrins.

Tetrabenzoporphyrins have been extensively studied for their optical properties, especially in the emerging fields of photodynamic therapy and organic electronic devices [10]. Their macrocyclic architecture potentially combines the best features of both porphyrins and phthalocyanines in terms of light harvesting, stability and processability, thus making them interesting for a wide series of organic and optolectronic devices including DSSCs. The presence of carbon atoms available for substitutions on the *meso* positions allows to insert electron-donor and -acceptor groups that interact with the inner core of the macrocycle, leading to effective modifications of the molecular frontier orbitals. Nevertheless up to now very few examples have been reported due to the synthetic complexity of this class of compounds[11].

The novel zinc tetrabenzoporphyrin presented here, hereafter referred to as **PETBP**, is modified through the insertion of three phenyl groups which occupy all the *meso* positions of the aromatic porphyrinoic ring but one, both increasing the solubility of the molecule and reducing the occurrence of aggregation phenomena. The last *meso* position has been substituted by an ethynylbenzoic unit as anchoring group in order to create a D-π-Asystem, which enhances the electron injection into the titanium dioxide's conduction band and, in turn, the photocurrent in the solar cell. As already reported in the case of highly efficient porphyrins using the same anchoring group, the presence of a triple bond in the spacer increases the π-conjugation of the system and, together with the benzoic moiety, induces an axial character to the electronic distribution of the excited state. The combined action of such electron acceptor anchoring group with that of suitable spacers and electron donor groups yields a good geometry of the dye-semiconductor interface, with the molecule reasonably perpendicular to the TiO_2 surface and with photogenerated electrons and holes protected from direct recombination as well as favorably oriented towards the semiconductor and the hole transporter, respectively[12,13].**PETBP** could potentially be good candidate in BIPVs because of its expected higher chemical stability with respect to the related porphyrin structures and its intense green color.

Synthesis, characterization, redox and optical behavior of **PETBP** are presented in the following sections, and discussed in close relationship with ab initio results and with performance tests of **PETBP** used as dye in a DSSC framework.

Experimental

All reagents were obtained from commercial source, Aldrich, Fluka or CarloErba. The solvents employed in all the reactions discussed below were anhydrous and distilled before use: CH_2Cl_2 was distilled over calcium hydride; THF was treated with KOH and distilled over sodium under argon, using benzophenone as a visual indicator. Reactions were monitored by Thin Layer Chromatography (TLC) employing a polyester layer coated with 250 mm F254 silica gel. The purification of compounds was performed by column chromatography using silica gel Carlo ErbaReactifs SDS 60A C.C. 35–70 mm or cellulose (Avicel Cellulose microcrystalline, Merck.) with several mobile phases. For the spectroscopic measurements the transparent semiconductor thin films were prepared by blade casting a nanocrystalline paste of either TiO_2 (SolaronixTi-Nanoxide HT) or ZrO_2, followed by drying and sintering a 450°C for 30 min. ZrO_2 paste was obtained as reported in[13]. Sensitization of semiconductor thin films was performed by dipping in a ~10^{-4} M solution for at least 6 hours.

Synthesis

Triphenyl-tetrabenzoporphyrinateZn(II) complex **(1)** and 4-ethynylmethylbenzoate were synthesized according to previously published procedures [14,15].

5,10,15-(triphenyl),20-(bromo)tetrabenzoporphyrinate Zn(II) (2). In a typical procedure, 200 mg of **(1)** were dissolved in 4 ml of dichloromethane and then 44 mg of N-bromosuccinimide and 1 ml of pyridine were added. The mixture was allowed to react for one hour at room temperature, then HCl 1N was added to it and the resulting solid was filtered, washed thoroughly with water and dried to constant weight. It was used in the next synthetic step without further purification.

5,10,15-(triphenyl),20-[ethynyl-(4-carboxymethyl)phenyl]tetrabenzoporphyrinate Zn(II) (3). 100 mg (0.11 mmol) of (2) were dissolved in 4 ml of ethanolamine and 2 ml of anhydrous THF and stirred under nitrogen with an excess of 4-ethynylmethylbenzoate (53 mg,

0.33 mmol), 17.5 mg (0.022 mmol) of $Pd(PPh_3)_2Cl_2$ and 2.1 mg (0.011 mmol) of CuI. The mixture was allowed to react for 24 hours at 60°C in nitrogen atmosphere, then was concentrated and treated with HCl 1N. The resulting solid was filtered, washed with water and purified by column chromatography, using cellulose as stationary phase and petroleum ether:THF as mobile phase. (53 mg, 50% yield), IR (neat, cm^{-1}, 2340, 1755), UV-Vis (CH_3CN, 456, 648 nm); ^1H NMR (THF d8, ppm): δ =3.70 (s, 3H, OCH_3), 7.40-7.46 (m, 12H, aromatics), 7.50-7.56 (m, 12H, aromatics), 7.66-7.71 (m, 9H, aromatics), 7.74-7.75 (m, 2H, *p*-ethynylbenzoate), 7.79-7.80 (m, 2H, *p*-ethynylbenzoate);MALDI-TOF (m/z) $[M^+H^+]$ 961.2; elemental analysis: calcd. C= 80.04%, H= 3.99%, N= 5.83%; found. C= 79.81%, H= 3.70%, N= 5.53%

5,10,15-(triphenyl),20-[ethynyl-(4-carboxy)phenyl]tetrabenzoporphyrinate Zn(II) (PETBP).

21 mg (0.022 mmol) of (3) were dissolved in 5 ml of a 1:1 THF-methanol solution and hydrolyzed with the addition of 190 mg of NaOH dissolved in 5 ml of H_2O. The resultant mixture was refluxed under stirring until the TLC showed the complete disappearance of the reagent. Then it was concentrated to eliminate THF and methanol and the resulting aqueous phase was acidified with HCl 1N to allow the precipitation of the product which was collected by filtration and washed several times with water. The resulting 25 mg of crude were purified by column chromatography using cellulose as stationary phase and 4:1 hexane:THF and 1:1 chloroform:methanol as mobile phases. The green solid obtained was washed several times with water and methanol. (14 mg, 70% yield); IR (neat, cm^{-1}, 3354, 2343, 1722), UV-Vis (CH_3CN, (ε_{456} $7.73x10^4$, ε_{650} $2.96x10^4$);^1H NMR (THF d8, ppm): δ = 7.51-7.80 (m, 31H, aromatics), 7.85-7.90 (m, 2H, *p*-ethynylbenzoic), 7.94-7.98 (m, 2H, *p*-ethynylbenzoic);MALDI-TOF (m/z) $[M^+Na^+]$ 967.120; elemental analysis:calcd. C= 79.95%, H= 3.83%, N= 5.92%; found C= 79.35%, H= 3.57%, N= 5.47%

Characterizations

Infrared spectra were recorded on a Shimadzu FT-IR Prestige-21 spectrometer in KBr pellets, in nujol mull or as powder by an attenuated total reflectance (ATR) unit.

UV-vis spectra were recorded in transmission on a Perkin-Elmer Lambda 950 UV-vis/NIR spectrophotometer for both solutions and transparent sensitized films.The ^1H NMR spectra were recorded in THF-d_8 at 27 °C on a Bruker AVANCE 600 NMR spectrometer operating at a proton frequency of 600.13 MHz;chemical shifts (δ) are given in ppm relative to the residual solvent peak of the THF-d8 solvent (3.58, 1.73 ppm).Mass spectra have been recorded at Toscana Life Science facility in a MALDI-TOF/TOF Ultraflex III (Bruker) by MALDI-TOF method (α-cyano-4-hydroxycinnamic acid (HCCA) as matrix). Isotopic pattern simulations have been performed by Bruker Daltonic program.

Steady-state fluorescence spectra for dye solution and sensitized films (TiO_2 and ZrO_2) were recorded in a JobinYvon Fluorolog3 spectrofluorometer, using grids of 5 nm for the excitation and 5 nm for emission. Time-resolved fluorescence measurements were carried out by a time-correlated single-photon-counting (TCSPC) system (Horiba-Jobin-Yvon). Time-resolved measurements were carried on exciting the samples using a 405 nm pulsed laser diode and collecting the emission decay at the corresponding maximum emission wavelength for the analyzed dye. The fluorescence decay profiles were analyzed through decay analysis software (DAS6a HORIBA Scientific) to a multiexponential decay equation. The quality of the fits was checked by examining the residual distribution and the χ^2 value.

Cyclic voltammograms were recorded at 25 °C with a potentiostat-galvanostatMetrohmPGStat 204 in a conventional three electrodes cell, a platinum disk (∅1mm) was used as working electrode together with a platinum wire as auxiliary electrode. The reference electrode was $Ag/AgNO_3$ (0.01M) in distilled acetonitrile (ACN) (Aldrich) (E_0 vs SCE = 0.298 V[16]) and the Fc^+/Fc (ferrocenium/ferrocene) couple was used as external standard. The samples solutions were ~10^{-4}M in distilled anhydrous solvents and dry tetra(*n*-butyl)ammonium tetrafluoborate (TBATFB) (Aldrich) was used as the supporting electrolyte at 0.1 M. The solutions were previously purged 10 minutes with nitrogen and all measurements were performed under nitrogen. Cyclic voltammetry (CV) investigations were carried out at scan rates typically ranging from 0.05 to 2 Vs^{-1}.

The DSSC devices have been prepared according to the following procedure: as substrate a KINTEC FTO (resistivity: 15 ohm/sq) has been employed, the photoelectrode has been prepared using Dyesol DSL 18NR-T + scattering layer by Solaronix, with an active area of 0.20 cm^2 and dipped in a 0.2 mM dye solution in acetonitrile for 14h; the counter-electrode has been prepared by Electron Beam deposition of a 50 nm-thick Platinum film; the electrolyte solution was composed of 0.1 M LiI, 0.03 M I_2, 0.6 M 1-methyl-3-propylimidazolium iodide, and 0.5 M, *t*-butylpyridine in acetonitrile. To evaluate the effect of possible aggregation phenomena, different quantities of chenodeoxycholic acid (CDCA) have been added to the dye solutions. Photocurrent-voltage measurements were performed using a Keithley unit (Model 2400 Source Meter). A Newport AM 1.5 Solar Simulator (Model 91160A equipped with a 1000 W xenon arc lamp) served as a light source. The light intensity (or radiant power) was calibrated to 100 mW cm^{-2}using as reference a Si solar cell.The incident photon-to-current conversion efficiency (IPCE) was measured by the DC method, using a computer-controlled xenon arc lamp (Newport, 140 W, 67005) coupled with a monochromator (Newport Cornerstore 260 Oriel 74125). The light intensity was measured by a calibrated silicon UV-photodetector (Oriel 71675), and the short circuit currents of DSSCs were measured by using a dual channel optical power/energy meter, (Newport 2936-C).

Computational Details

Two parallel series of calculations have been performed to elucidate the ground- and excited-state properties of the **PETBP** molecule. A first batch of DFT and TDDFT calculations has been carried out by using the ORCA suite of programs [17] in a localized-basis-set framework. In detail, the Kohn-Sham orbitals have been expanded on a def2-TZVP Gaussian-type basis set[18,19]. The same def2-TZVP basis has been also used as an auxiliary basis set for Coulomb fitting. The molecular geometry has been fully optimized at the B3LYP level of theory[20,21], also including dispersion forces calculated by using the DFT-D3 approach[22] with the Becke-Johnson damping[23-25]. Solvation effects have been included in ground- and excited-state calculations by applying the conductor like screening model (COSMO)[26]. A second batch of DFT calculations have been performed by using the Quantum ESPRESSO suite of programs[27] in a plane-wave pseudopotential framework. In detail, the molecule has been accommodated in a large (60 a.u.^{3}) periodic supercell and its geometry has been fully minimized at the same B3LYP level of theory and by using the DFT-D2 method to simulate dispersion forces[28]. Satisfactorily converged results have been obtained by using norm-conserving pseudopotentials[29] and an 80 Ry (320 Ry) cut-off on the plane wave representation of Kohn-Sham orbitals (electronic density). The vacuum level of the periodic system has been calculated by using the Makov-Payne method[30] in order to compare the results of GTO and PW calculations, characterized indeed by negligible differences. The periodic framework has been employed to simulate low energy excited states of the molecule, approximated by using open-shell constrained B3LYP calculations. Such calculations provide information of charge displacements under optical absorption of **PETBP**.

Results and Discussion

Synthesis

According to what reported elsewhere[31], tetrabenzoporphyrins can be synthesized by following different methods: retro Diels-Alder, oxidative aromatization, one-pot cycloaddition approach with aromatization, one-pot Heck approach with aromatization and condensation of isoindole or other aromatic precursors. Some of these routes can lead to meso-substituted macrocycles while others can allow both meso- and β-substitutions. If we consider the synthetic paths proposed above it is clear that they all have the advantage of a fine tuning of the functional groups that can be inserted in the macrocyclic structure due to the fact that almost all the steps are performed in solution and in relatively mild conditions. The only harsh step is the possible final aromatization, which needs temperatures above 200°C and could lead to the loss of the most labile substituents. On the left hand, the disadvantages that all such methods show are related to the preparation of the macrocycle precursor(s), which are long, non-trivial and low-yielding. Moreover, the products obtained are generally symmetrically substituted even if asymmetric products can in principle be prepared at a price of a longer and more complicated synthetic process. Direct condensation of the aromatic precursors can be also considered as a possible alternative. We have chosen such procedure among different synthetic strategies leading to *meso*-substituted tetrabenzoporphyrins[14]. The reaction is a statistical condensation between phenylacetic acid and phthalimide in presence of zinc acetate at 360°C. As previously pointed out, this kind of synthesis is way less specific than other routes that have been developed more recently[32,33], and leads to a statistic mixture of meso-substituted macrocycles that have to be carefully separated from one another and from other by-products. More specifically, the drawback is that the use of such harsh conditions makes very difficult to control the reaction and leads to troublesome purification processes due to the formation of by-products, even if it allowsto obtain the desired product with a single synthetic step starting, in our case, from commercially available and low cost precursors. The synthesis of **PETBP** is reported in Scheme 1.

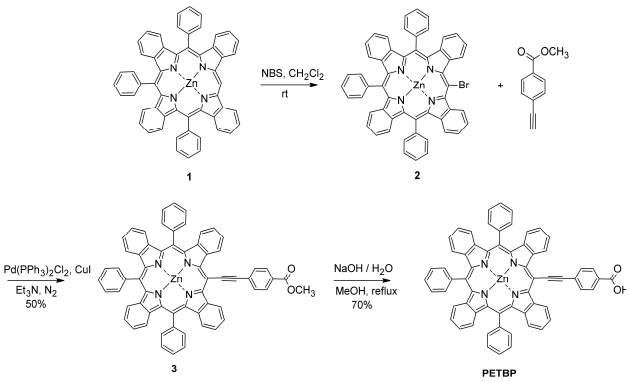

Scheme 1: Synthesis of **PETBP**

The starting compound **(1)** obtained as reported in literature is easily contaminated by traces of zinc tetraphenyl-tetrabenzoporphyrin which is nonreactive in the subsequent synthetic steps and can be easily removed during the related purification procedures, even if a small amount of such byproduct has sometimes been detected in the MALDI spectra of **(1)**. Once obtained, the desired triphenyl-tetrabenzoporphyrin was brominatedonto the only free meso-position of the macrocycle: this is a necessary preliminary step to the following Sonogashira coupling, which is performed with 4-ethynylbenzoate methylester and catalyzed by $Pd(PPh_3)_2Cl_2$ and CuI in an organic base such as triethylamine (TEA)[15]. The final synthetic step is the basic hydrolysis of the methylester group which restores the acidic functionality allowing the anchorage to the titanium dioxide surface. It is worth to remark that the bottle-neck reaction which lowers the total yield of the synthetic pathway is the synthesis of the precursor **(1).** At the end of the synthetic path a green solid powder, stable to air and easy to handle, has been isolated. The stoichiometry and structure of the obtained compound

has been verified by elemental analysis, which gave carbon, nitrogen and hydrogen percentages compatible with the calculated ones. MALDI measurements confirm the molecular weight of **PETBP** showing an intense signal having a mass-to-charge ratio of 967.120 which corresponds to the radical cation plus a sodium ion. The IR spectrum contains the expected diagnostic bands assigned to the stretching of aromatic CH bonds, of the triple bond and of the -COOH carbonyl group, centred at 3354, 2343 and 1722 cm^{-1} respectively. The UV-Vis measurements of the final product will be described in detail in the next paragraph.

Uv-vis spectroscopy

The UV-vis spectrum of **PETBP** in acetonitrile is shown in figure 1.As clearly visible in the figure, it is characterized by a very intense Soret band peaked at 456 nm and by a less intense Q band peaked at 655 nm, as usual in porphyrin spectra. The extension of the aromatic core,to the four benzene rings fused onto the benzoporphyrin macrocycle is expected to produce a drastic lowering of the energy of the electronic π-π^* transition with respect to porphyrins.

As an example, the comparison between the spectra of zinc tetraphenyl-porphyrin (Zn-TPP) and zinc tetrabenzoporphyrin shows that the Soret and Q band of the latter one are both red-shifted (433 vs 423; 631 vs 548 nm)[34,35]. Moreover, the introduction of phenyl substituents in the *meso* positions produces a further bathochromic shift as reported for the spectrum of zinc tetraphenyl-tetrabenzoporphyrin (445 nm/656 nm)[36].

PETBP holds three phenyl groups and the ethynylbenzoic moiety onto the *meso* positions of the tetrabenzoporphyrins core, its spectrum is quite typical for such kind of macrocycle and the unsymmetrical substitutions result only in a slight red-shift of the Soret band.

Both absorption bands are sharp enough to indicate that possible aggregation phenomena in solution are not relevant in the present conditions. The occurrence of more than one absorption bands in the visible region of the spectrum is a promising feature because it can improve the harvesting of solar radiation.Both the Soret and Q bands are still present in the absorption spectrum of the dye anchored to TiO_2. Although their shapes are slightly broader than the corresponding bands in solution, no significant wavelength shifts are found. Band broadening of a dye loaded on a semiconductor thin layer may be generally due to the scattering effect of the films or to the molecular aggregation. Both effects seem to be negligible in our case even if molecular aggregation is very common in this class of dyes. As discussed below, this could be one of the effects of molecular distortion in **PETBP**.

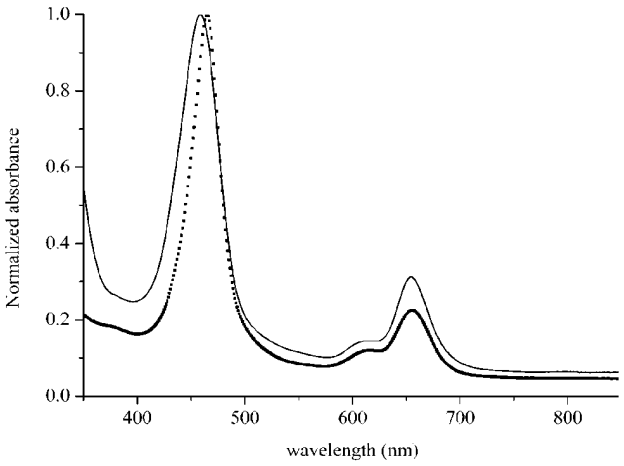

Figure 1: normalized spectra of **PETBP** in acetonitrile solution (solid) and onto TiO_2 (dotted).

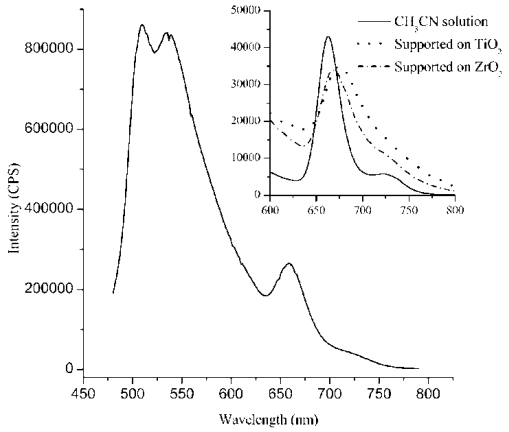

Figure 2: Emission spectrum (λ_{ex}= 460 nm) of **PETBP** in acetonitrile; inset: emission spectra (λ_{ex}= 470 nm, cutoff filter at 600 nm) in solution and as thin films on TiO_2 and ZrO_2.

Fluorescence measurements

The fluorescence properties of **PETBP** have been studied in solution and with the molecule bonded to TiO_2 and ZrO_2 films, in order to estimate the yield of charge injection into the semiconductor conduction band and, in turn, the occurrence of an effective photovoltaic effect in a DSSC device. Measuring the quenching of the supported dye emission is a relatively straightforward qualitative method to estimate its ability to inject photogenerated electrons into the empty electronic states of TiO_2.The measurement is performed by comparison with a semiconductor substrate where charge injection is forbidden for energetic reasons: ZrO_2 is often chosen as an electro-optically inert substrate because its conduction band edge, significantly higher than that of TiO_2, is energetically out of reach by the lowest-energy excited state of most dyes. Moreover, ZrO_2 can be obtained in reasonably transparent films, thus minimizing scattering interferences during emission measurements. Its surface chemistry is also similar to that of TiO_2, resulting therefore in a similar dye loading when the samples are prepared in the same conditions.

The emission spectrum of the molecule dissolved in acetonitrile, shown in figure 2, has been registered at λ_{ex} = 460 nm and consists of two bands. The intense emission around 500 nm is ascribed to the Soret band ($S_2 \rightarrow S_0$), in agreement with the well established behavior of tetrabenzoporphyrins

having low atomic weight, d^{10} central metal ions and no "dark" (i.e. charge transfer, d–d or n-π*) electronic states interleaved between S_2 and S_1 states[37].The shape of this strong and broad band appears influenced by the experimental conditions being the multiple vibration levels of the electronic transition more or less resolved (see fig S1). The fluorescence from this band can also be interpreted in the light of the computational data of which we anticipate here the result relative to absorption of the Soret band that is being provided by two main transitions (see below).

The emission from the Q band ($S_1 \rightarrow S_0$) has been found to have its maximum at 663 nm, with a Stokes' shift of 8 nm.

The emission spectra of TiO_2 and ZrO_2 sensitized films, measured at λ_{ex} = 470 nm, are shown in the inset of figure 2 and compared with the one in solution. They are in a general good agreement and, as expected, their shapes (with maxima respectively found at 675 and 668 nm) appear broadened, likely due to the partial formation of aggregates, and red-shifted if compared to that found in solution. Both relative emission intensity values are quite high when compared with those measured in solution and even if it is impossible to directly compare the difference among the spectra, this suggests a high loading of molecules onto the semiconductor surfaces.

Time-correlated single photon counting measurements of the 660 nm emission ($S_1 \rightarrow S_0$) have been performed with a laser beam having λ_{ex} = 405 nm, which directly excites the Soret band ($S_2 \rightarrow S_0$) and hinders the kinetic discrimination between the two decays ($S_2 \rightarrow S_0$, $S_1 \rightarrow S_0$), being the relaxation time a linear combination of both phenomena. As a consequence, a quantitative estimate of the external quantum efficiency of the only S_1 decay is difficult, even if some qualitative information can be still obtained by analyzing the curves shown in figure 3.In this regard, both the measurements of sensitized titania and zirconia surprisingly show a significant quenching, if compared with the solution measurements, that can be attributed to intermolecular recombination processes, although the absorption spectra shown in figure 1 do not show any relevant aggregation of the molecules. At any rate, the excited state of the system evolves faster in the case of titanium dioxide than of zirconium dioxide(Table I), thus indicating the occurrence of an effective transfer of the photogenerated charge towards the suitable electronic states

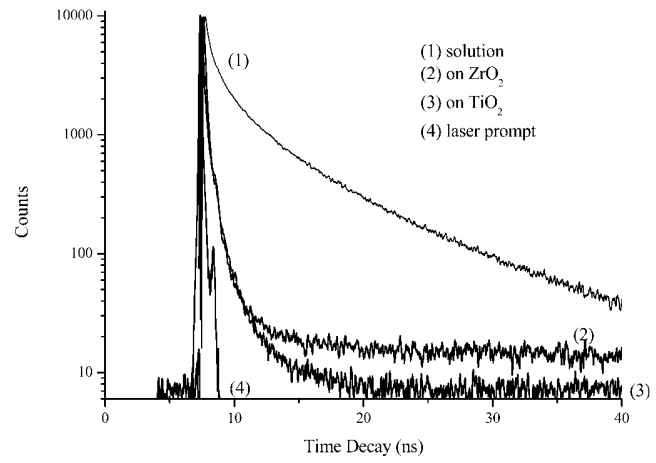

Figure 3: Fluorescence kinetics of (1) **PETBP** solution, (2) sensitized ZrO_2 system, (3) sensitized TiO_2 systems.

Table I: Photophysical and electrochemical propertiesof **PETBP**

λ_{max}[a][nm]	λ_{em}[a][nm]	$\tau_{S_1}^b$ [ns] ACN	$\tau_{S_1}^b$ [ns] TiO_2	$\tau_{S_1}^b$ [ns] ZrO_2	$E_{1/2}$[c] [V]	$E_{(0\text{-}0)}$[d] [eV]	$E_{(s^+/s^*)}$[e] [V]
456(B) 655(Q)	~500$_{(S2\rightarrow S0)}$ 663$_{(S1\rightarrow S0)}$	6.5	0.09	0.12	0.53	1.88	-1.35

[a]Absorption and emission data in acetonitrile solution;[b]Lifetimes values in solution and sensitized films (see SI for details);[c]Ground state oxidation potential versus SCE;[d]0-0 transition energy estimated from the intercept of the normalized absorption and emission spectra;[e]Estimated LUMO energyvs SCE from the estimated HOMO energies (ground state oxidation potential) andthe 0-0 transition energies.

in the titania substrate, as confirmed by IPCE spectrum.

Redox behavior

The redox properties of **PETBP** solvated in acetonitrile have been investigated by cyclic voltammetry. The corresponding cyclic voltammogram is shown in figure S2.

Three one-electron quasi-reversible oxidations and one irreversible reduction are visible in the range of explored potentials. The first oxidation potential is centered at 0.53 V vs SCE while the first reduction potential (at the maximum of reduction wave) at -1.13 V vs SCE. Such values yield a 1.66 V vs SCE electrochemical band-gap of **PETBP**. This behavior is consistent with that generally observed in the case of macrocyclic compounds non containing electroactive metals and characterized by redox processes involving the organic part of the molecule only.

The extension of the π-conjugation and the *meso* substitution of the porphyrin ring is expected to reduce the first oxidation potential due to the stronger stabilization of positive charges, in parallel with a red-shift of the Q band in the absorption spectrum. It is not always predictable whether the former modification has a stronger effect than the latter one. To give an example which concerns similar macrocycles[38-40], the zinc tetrabenzoporphyrin Zn-TBP[40](0.36 V vs SCE) is more easily oxidized than zinc tetraphenylporphyrin Zn-TPP(0.75V vs SCE)[39]. Moreover, the insertion of aryl groups in the *meso* positions modulates the oxidation potential in diphenyl-

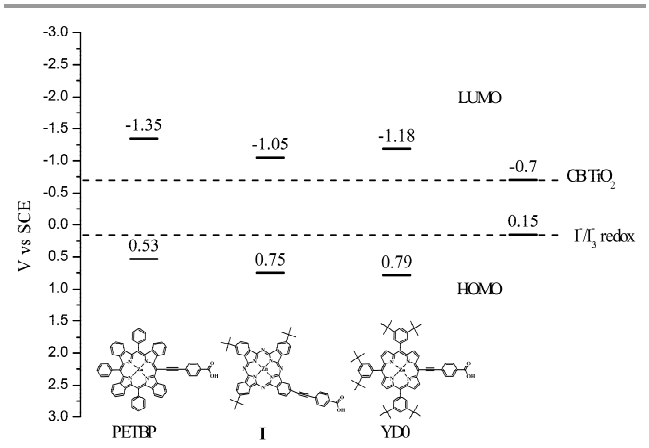

Figure 4: Schematic energy-level diagram of **PETBP**, **I**[43] and **YD0**[42] in respect of TiO_2CB and redox mediator. (In this context "HOMO" and "LUMO" terms are formally improper, but commonly accepted).

tetrabenzoporphyrins[35] or tetraphenyl-tetrabenzoporphyrins[40] which is placed at an intermediate value between TPP and TBP.

PETBP shows oxidation and reduction potentials consistent with the above reported values, with the electron-withdrawing effect of the ethynylbenzoic group linked to the core of the macrocycle evidently favoring the reduction process.The measured first oxidation potential of **PETBP** permits the localization of the ground state potential (S^+/S) of the compound and, together with the 0-0 optical transition energies, obtained by the intersection of the normalized lowest energy absorption peak and highest energy fluorescence peak, gives the energy level of the singlet excited state of **PETBP**, according to the equation: $E(S^+/S^*) = E(S^+/S) - E(0\text{-}0)$[41]. In table I all the photophysical and electrochemical characteristics have been gathered. Figure 4 shows a schematic energy diagram of **PETBP** compared with those of two similar dyes for DSSC, namely the zinc porphyry in **YD0**[42] and zinc phthalocyanine **I**[43], which can be considered the structurally phthalocyanine and porphyrin analogous of **PETBP**.The tetrabenzoporphyrin species has the lower oxidation potential, having at the same time the S/S^- potential properly located well above the CB of TiO_2, and granting a relevant driving force to the charge injection, and the S/S^+ potential suitably positioned under the redox mediator I^-/I_3^- potential, even if not optimally placed for an efficient reduction of the photooxidized dye.

Ab initio results

Ab initio simulations have been carried out to investigate the effect of substituents on the charge-density distribution of **PETBP**, both in its ground state and low-energy excited state, to gain insight into the charge transfer process to the semiconductor that involves the photoexcited dye.

The **PETBP** molecular structure has been optimized at the B3LYP level of theory, as isolated system in gas phase as well as in ethanol and acetonitrile solutions, modeled by using the COSMO approach. The stable geometry of the molecule is shown in figure 5.In all these cases the benzo- groups show a relevant bending, sketched in figure 5, due to the repulsive interaction between the π-electron rich phenyl- and benzo-groups. A similar bending is not observed in the case of the Zn-TBP, which is strictly planar, neither in the case of the Zn-TPP, in which the phenyl groups are twisted with respect to the planar macrocycle. The same bending is found instead in the case of the Zn- tetraphenyl-tetrabenzoporphyrin molecule, so that we can safely state that it does not depend on the insertion of the anchoring ethynylphenyl group. The drastic lowering of the typical C_4- or D_4-like symmetry of the porphyrin archetypical structures induced by the combined effect of the bending and the anchoring group affects the electronic properties of the ground and excited molecular states. Regarding the **PETBP** ground state, the energy position with respect to the vacuum level and the spatial distribution of the B3LYP frontier orbitals are shown in figure 6. The idealized

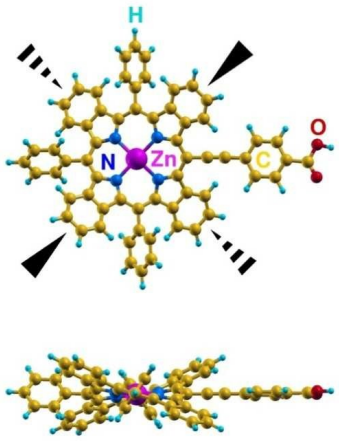

Figure 5: Top and side views of the optimized structure of the **PETBP** molecule.

distribution of frontier orbitals of a C_{4v} or D_{4h} molecule (one fully symmetric HOMO and a double degenerate LUMO) is strongly perturbed, even if not entirely broken. We note, in particular, a moderate 0.3 eV splitting of the two components of the E-type LUMO (LUMO and LUMO+1 in the figure), due to effect of the electron-attractor ethynylphenyl group, which is significantly involved in several frontier orbitals.

Such a perturbation affects also the excited states of the molecule and limits the application of the early Gouterman's four-orbital model[44,45], which successfully predicted the inherent multi-orbital nature of the optical absorption in porphyrins.

In detail, the absorption spectra of symmetric porphyrins were described in terms of a multi-particle basis formed by the HOMO-1, HOMO and double-degenerate LUMO (four orbitals), combined to yield a low frequency transition, forbidden via electric dipole and therefore often very weak (Q band), and a high-frequency very intense transition (Soret band). Let us consider now the absorption spectrum of the **PETBP** molecule in an up-to-date ab initio TDDFT framework. The TDDFT absorption spectrum of the molecule solvated in acetonitrile (by using the COSMO model), calculated at the B3LYP level of theory, is shown in the right panel of figure 6.The occurrence of a weak Q band and a strong Soret band, peaked at 1.95 eV (634 nm) and 2.91 eV (427 nm), is in agreement with the Gouterman's model and with the **PETBP** spectrum measured in similar conditions (see figure 2). The position of Casida's eigenvalues (i.e., the TDDFT transition energies), and the projections of the corresponding Casida's eigenvectors on the basis of the B3LYP frontier orbitals are represented by colored sticks below the absorption spectrum and by colored arrows connecting orbitals in the left panel[46]. The contribution of a single orbital-orbital transition to the absorption is marked by a number indicating the fractional contribution of the

Journal Name

ARTICLE

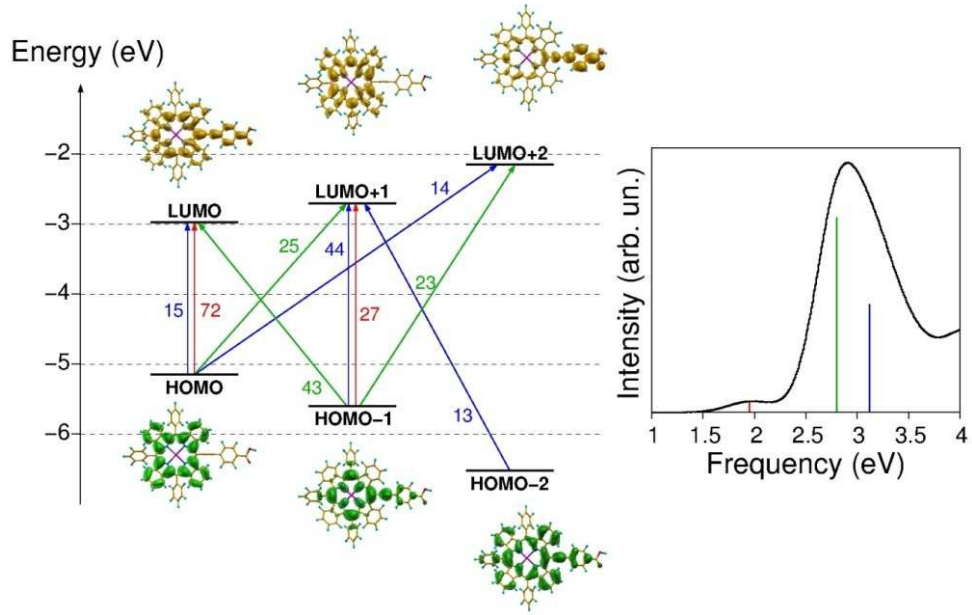

Figure 6: Left panel: Energy alignment of Kohn-Sham eigenvalues of **PETBP** calculated at the B3LYP level of theory, accompanied by the corresponding $|\Psi|2$ spatial representations. Right panel: TDDFT absorption spectrum of the molecule, also calculated at the B3LYP level of theory. The spectrum has been obtained as a convolution of Gaussian functions (fwmh=0.5 eV) centred on the first 100 transitions, calculated by using a polarizability basis of 1000 vectors. Three main transitions, discussed in the text, are represented by a red, a green and a blue stick below the spectrum. The projections of such transitions on the basis formed by the connection between occupied and unoccupied B3LYP Kohn-Sham orbitals are represented by colored arrows in the left panel, with contributions from single orbital-orbital transition to the absorption marked by numbers indicating the fractional contribution of the transition to the absorption.

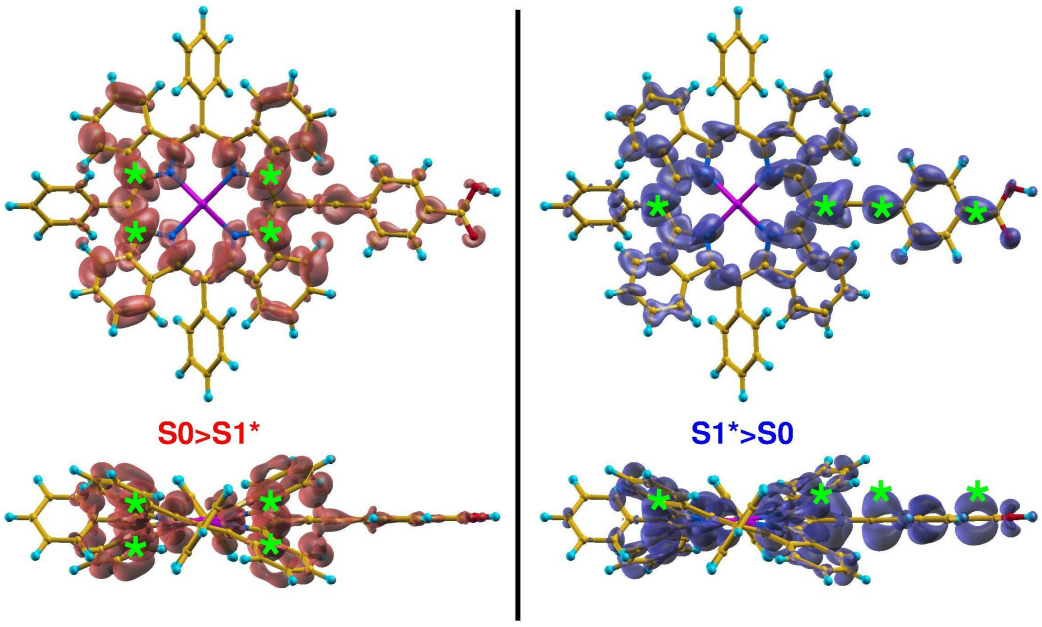

Figure 7: Charge-density maps showing the difference between the total density of the ground state (S_0) and the first singlet excited state (S_1*). Blue (red) isosurfaces enclose regions where the electronic density of S_1* is higher (lower) than that of S_0. Green stars indicate regions of particular accumulation (depletion) of charge, and are discussed in the text

transition to the absorption. We note that the symmetry breaking occurred in the molecule is connected to the predominant (72%) HOMO→LUMO character of the Q band (red stick), even if there is still a significant (27%) contribution from the HOMO-1→LUMO+1 transition (red arrows). The Soret band is instead characterized by two main intense transitions (green and blue sticks) still composed by a complex web of single-particle excitations involving the macrocycle as well as the anchoring group (green and blue arrows).Further information about the nature of the S_0 and S_1* states is provided by an approximate spatial representation of the charge displacement which characterize the $S_0 \rightarrow S_1$* excitation, obtained by performing a constrained-DFT open-shell simulation of the S_1* excited state at the B3LYP level of theory. The charge density of the excited state has been calculated by using the ground-state optimized structure and then subtracted from the charge density of the ground state, with the corresponding charge density maps shown in figure 7.In order to facilitate the understanding of displacement patterns the figure has been divided in two parts: the blue (red) isosurfaces in the left (right) part enclose regions where the charge density of the S_1* excited state is higher (lower)than the charge density of the S_0 ground state. In other words, the charge density flows from the red regions to the blue regions when the molecule is excited from S_0 to S_1*. The charge-transfer pattern is quite complex, and deserves to be discussed in detail. First of all, a larger displacement of charge involves, as expected, the π-conjugated orbitals mainly located below and above the molecular backbone. Regions more involved in such π displacement have been indicated by stars in figure 8. The displacement is mainly driven by the presence of the electron-withdrawing ethynylbenzoic group. A relevant amount of electronic charge is transferred upon excitation from four C atoms belonging to the inner macrocycle (stars in the right panel of figure 7), and from the four benzene rings (minor contributions) to the ethynylbenzoic group and to two *meso* C atoms aligned to it (stars in the left panel of figure 8): as a result, charge in the excited state is axially oriented toward the anchoring group.

The absence of a strong electron-donating group as aryl-amino moieties, often employed in such kind of D-π-A molecular architecture, does not allow for a stronger polarization of the molecular excited state: the phenyl groups which saturate the remaining *meso* positions take in fact negligible part in the excitation of the molecule to the S_1* state. As a significant secondary detail, we also note that a complementary displacement of σ charge involves regions affected by π displacement. This is particularly visible in the case of the fully planar ethynylbenzoic group, where an accumulation of π charge in the excited state is clearly accompanied by a depletion of σcharge (the complementary red spots in the plane of C atoms), but the same kind of "sigma rebound" can be found in the case of all the atoms involved in the π-displacement, as previously found also in the case of smaller π-conjugated molecules[47,48].

Finally, we have estimated the reduction and oxidation potentials of the molecule as the electron affinity and ionization potential, respectively, of the acetonitrile-solvated **PETBP**. The calculated values (-1.3 V and 0.5 V) nicely agree with the measured potentials discussed above, and confirm that a consistent potential drop (~0.6 V) drives the transfer of excited electrons from the molecule to the TiO_2 conduction band (-0.7 V).

Table II: Photovoltaic parameters for DSSCs based on **PETBP**.

Dye	CDCA [mM]	η [%]	V_{OC} [V]	J_{SC} [mA/cm^2]	FF
PETBP	0	0.95	0.493	2.80	0.69
	5	1.27	0.551	3.33	0.69
	10	2.22	0.577	5.83	0.66
N719	0	7.51	0.772	14.32	0.68

Photovoltaic performances

All the experimental data collected on **PETBP** fulfill most of the theoretical requirements a photosensitizer should possess to be processed in a dye-sensitized solar cell. Its photovoltaic properties have been therefore tested in photoelectrochemical devices.

Due to the electronic distribution of the macrocycle and of the ethynylphenyl spacer, a fast intramolecular charge transfer should be expected as well as an unfavorable π-π stacking during the uptake process, which may lead to intermolecular quenching or back transfer of the injected electrons. As widely

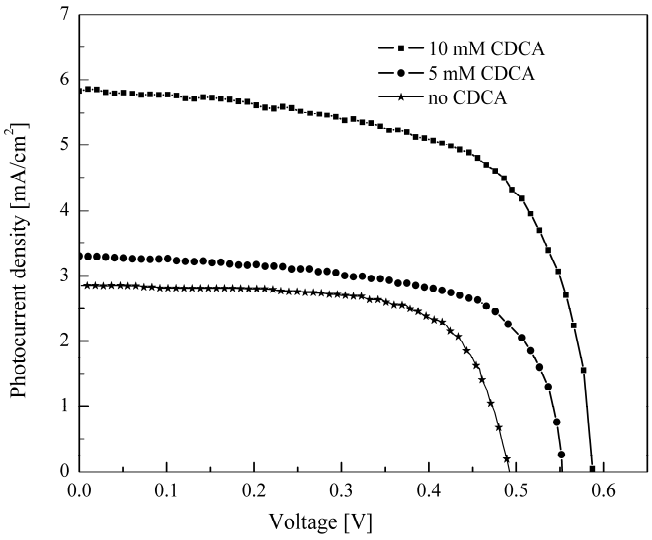

Figure 8: I/V plot of cells based on **PETBP** with different amounts of CDCA

reported in literature, co-adsorbers(like CDCA) are added to the dye bath, resulting helpful for many organic and metal complexes dyes. CDCA can occupy spaces between dye molecules and can assist favorable packing of dye molecules by avoiding aggregation. Moreover, CDCA, being co-adsorbed with the dyes onto TiO_2, shields the semiconductor surface against the recombination process, thus suppressing the dark current[49-51]. The reduction of unfavorable recombination phenomena leads to an enhancement of both Jsc and Voc, often observed for devices fabricated in the presence of CDCA. In fact, even in our case, the dark current measurements performed on devices prepared with and without CDCA, reported in figure S3, show that the onset of the dark currents moves from around 0.4 V without CDCA to around 0.5 V upon the introduction of CDCA in the dye bath. Since both devices were fabricated and tested in the same conditions, only the sensitizer/TiO_2 interface influenced this parameter; therefore we can deduce that the improvement of Jsc and Voc observed for PETBP dye in the presence of CDCA could be attributed to the suppression of the back electron transfer from the conductive oxide to the electrolyte carried out by the PETBP-CDCA system.

On these basis, the use of chenodeoxycholic acid (CDCA) as coadsorbent was implemented for the fabrication and the test of the **PETBP**-based DSSC.

We prepared 0.2 mM solutions of **PETBP** dye in acetonitrile with variable CDCA concentrations (0, 5 and 10 mM) and studied the influence of the amount of additive on photovoltaic parameters, which are shown in Table II.

By competing with the dye for the binding on the titania surface, the CDCA minimized detrimental dye aggregation effects. Moreover, the use of the co-adsorbent ensured a uniform coverage of the inorganic semiconductor, thereby lowering the probability of recombination between injected electrons with I_3^- and other acceptor species.

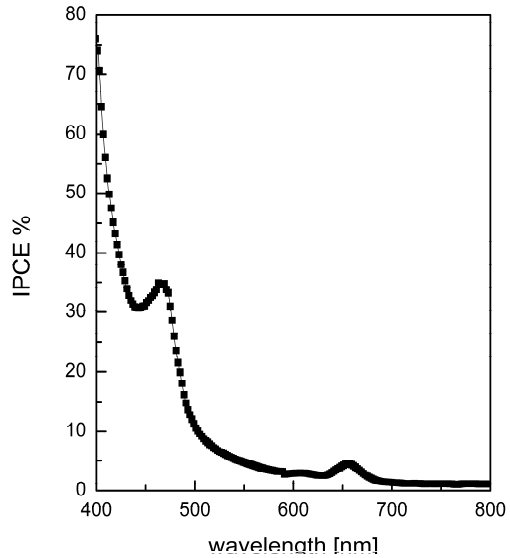

Figure 9: IPCE spectrum for of a DSSC based on **PETBP**with 10 mM CDCA.

The I-V curves of DSSCs based on **PETBP** dye, in the presence of different amount of CDCA, are shown in figure 8 while in figure 9 the incident photon to current spectrum (IPCE) is showed for the cell with 10 mM coadsorber. This conversion efficiency plot resulted in agreement with the light-harvesting range of sensitizer, showing a maximumof ~35% at 470 nm and a very weak (~4%) signal at 655 nm. Thissuggests that the electronic transitions associated to the Soret band are suitable for the production of photogenerated electrons and contribute most to the photovoltaic efficiency.

Conclusions

The synthesis of a new Zn-benzoporphyrin molecule has been performed and thoroughly discussed. Its electrochemical and optical properties have been also investigated and discussed in close relationship with ab initio studies aimed at clarifying its ground- and excited-state properties and at estimating the electronic distribution of its frontier orbitals. The alignment of the molecular orbitals of **PETBP** to the conduction band edge of TiO_2 and the I^-/I_3^- couple results to be suitable for the constraints required by the fabrication of solar devices and the molecule yields a maximum photovoltaic efficiency of 2.22%. The reasons for such a low performance are found in the non optimal position of the oxidation potential of **PETBP** with respect to the redox mediator potential, which is expected to negatively affect the dye regeneration process. Ab initio simulations show indeed that the electronic distribution of the excited state is suitable for an efficient charge transfer of photogenerated electrons to the semiconductor and suggest that the insertion of a stronger electron-donating group in an opposite position would enhance the charge flow and the photosensitizing performances of the dye. Moreover, aggregation patterns between the molecules and the consequent intermolecular electronic coupling are significant drawbacks that should be minimized through the optimization of the best admixture of dye and coadsorbent species in order to maximize the ratio between isolated molecules and molecular aggregates on the surface of TiO_2. The introduction of a strong electron-donor group in a suitable position, the study of the effect of the sensitization condition, the test of different redox mediators working at a higher potential than the iodide/triiodide couple, and the optimization of CDCA and other coadsorbent concentration are still under investigations because of the interesting possible exploitation of the intense green color of this new dye for building-integrated photovoltaics.

Acknowledgements

This work was supported by the CNR Italian Project EFOR-CABIR (Energia da FontiRinnovabili-FotovoltaiCoOrgAnico/IBridodITerzaGeneRazione) 2010-2014. Thanks to DrAnatoljSobolev for providing NMR measurements.

Notes and references

1 H.S.Jung, J.K.Lee,*J Phys Chem Lett*.,2013, **4**, 1682.
2 L.M Peter,*J Phys Chem Lett.*, 2011, **2**, 1861
3 E.Yoneda,M.K.Nazeeruddin, M. Grätzel,*J PhotopolymSci Technol.*, 2012, **25**, 175.
4 M.E. Ragoussi, M. Ince, T. Torres,*Eur J Org Chem*,2013,6475.
5 M.V.Martinez-Diaz, G.de LaTorre, Torres T.,*ChemCommun*. 2010,**46**,7090.
6 T.Bessho, S.M.Zakeeruddin, C.Y.Yeh, E.W.G.Diau, M. Grätzel,*AngewChemInt Ed*., 2010,**49**,6646.
7 A.Yella, H.W.Lee, H.N.Tsao, C.Yi, A.K.Chandiran, M.K.Nazeeruddin, E.W.G.Diau, C.Y.Yeh, et al.,*Science*. 2011,**334**,629.
8 M.E. Ragoussi, J.J. Cid, J.H. Yum,G. de la Torre, D. Di Censo, M. Grätzel, M.K. Nazeeruddin, T. Torres,*Angew Chem Int Ed*. 2012,**51**, 4375.
9 T. Ikeuchi, H. Nomoto, N. Masaki, M.J. Griffith, S. Mori, M. Kimura,*ChemCommun.* 2014,**50**,1941.
10 N.E.Galanin, E.V.Kudrik, G.P.Shaposhnikov,*Russ Chem Bull Int Ed.* 2008,**57**,1595.
11 R.Deshpande, B.Wang, L.Dai, L.Jiang, C.S.Hartley, S.Zou, H.Wang, L. Kerr, *Chemistry-An Asian Journal*, 2012, **7**,2662
12 V.K.Singh,R.K.Kanaparthi, L. Giribabu,*RSC Adv*. 2014, **4**, 6970.
13 A. Orbelli Biroli, F. Tessore, M. Pizzotti, C. Biaggi, R. Ugo, S, Caramori, et al.,*J Phys chem C*. 2011, **115**,23170.
14 K. Ichimura, M. Sakuragi, H. Morii, M. Yasuike, Y. Toba, M. Fukui, O. Ohno,*Inorganica Chimica Acta,* 1991, **186**,95.
15 S. Takahashi, Y. Kuroyama, K. Sonogashira, M. Hagihara,*Synthesis,*1980, 627.
16 V.V. Pavlishchuk, A.W. Addison, *Inorganica Chimica Acta*, 2000, **298**,97.
17 F. Neese, *WIREs ComputMol Sci*. 2012, **2**, 73.
18 A.Schäfer, H.Horn, R. Ahlrichs,*J Chem Phys*1992, **97**,2571.
19 F.Weigend, R. Ahlrichs,*Phys ChemChem Phys*2005, **7**,3297.
20 A.D. Becke,*J Chem Phys,* 1993, **98**,5648.
21 C.Lee, W.Yang, R.G.Parr,*Phys Rev B*. 1988, **37**,785.
22 S.Grimme, J.Antony, S.Ehrlich, H.Krieg,*J Chem Phys*. 2010, **132**,154104.
23 A.D.Becke, E.R.Johnson,*J Chem. Phys.,* 2005, **122**, 154101.
24 E.R.Johnson, A.D. Becke, *J Chem. Phys.*, 2005, **123**, 024101.
25 E.R.Johnson, A.D.Becke,*J Chem Phys.,* 2006, **124**, 174104.
26 S.Sinnecker, A.Rajendran, A.Klamt, M.Diedenhofen, F. Neese,*J Phys Chem A.*, 2006, **110**,2235.
27 P. Giannozzi, S. Baroni, N. Bonini, M. Calandra, R. Car, C. Cavazzoni, et al.,*J Phys Condens Matter*. 2009, **21,** 395502.
28 S. Grimme,*J Comput Chem*. 2006, **27**,1787.
29 N.Troullier, J.L.Martins,*Phys Rev B.*, 1991, **43**,1993.
30 G.Makov, M.C.Payne,*Phys Rev B.*, 1995, **51**,4014.
31 C.M.Brito Carvalho, T.J.Brocksom, K.T.de Oliveira. *ChemSoc Rev.*, 2013, **42**,3302.
32 O.S.Finikova, A.V.Cheprakov, I.P.Beletskaya, P.J.Carroll, S.A. Vinogradov,*J Org Chem*., 2004, **69**,522.
33 M.A. Filatov, A.Y. Lebedev, S.A. Vinogradov, A.V.Cheprakov,*J Org. Chem*., 2008, **73**, 4175.
34 G.H.Barnett, M.F.Hudson,K.M.Smith,*J ChemSoc Perkin Trans,*1975*, **1,** 1401**.**
35 D.S.Berezin, O.V.Toldina, E.V.Kudrik,*Russ.J GenChem* 2003, **73**,1309.
36 M. Gouterman,*The Porphyrins*ed. D. Dolphin, Vol.3, Academic Press,New York,1978, p. 1-156.
37 R.P.Steer,*PhotoChemPhotobiolSci*,2014, **13***,*1117.
38 Y. Madoka, Y. Tsiguo, O. Osami, I. Kunihiro, M. Hisayuki, S. Masako,*Inorganica Chimica Acta*, 1991, **185***,*39.
39 M.W.Renner, R.J Cheng, C.K.Chang, J. Fajer,*J Phys Chem*1990, **94**,8508.
40 A.Vogler, B.Rethwisch, H.Kunkely, J.Huettermann, J.O.Besenhard,*AngewChemInt Ed Engl*, 1978, **17**,951.
41 J.K.Park, H.R.Lee, J.Chen, H,Shinokubo, A,Osuka, D. Kim,*J Phys Chem C*,2008, **112***,*16691.
42 C.P.Hsieh, H.P.Lu, C.L.Chiu, C.W.Lee,S.H.Chuang, C.L.Mai, et al. *J Mater Chem*2010, **20***,*1127.
43 G. Zanotti, N. Angelini, A.M. Paoletti, G. Pennesi, G. Rossi, A. Amore Bonapasta, et al.,*Dalton Trans,*2011, **40**, 38.
44 M. Gouterman,*J MolSpectrosc,* 1961, **6***,*138.
45 M.Gouterman, G.H.Wagnière,*J MolSpectrosc,* 1963, **11***,*108.
46 M. Casida,*Recent advances in density functional methods,part I*, ed. P. Chong, World Scientific, Singapore, 1995, 155.
47 P. Bolognesi, G. Mattioli, P. O'Keeffe, V. Feyer, O. Plekan, Y. Ovcharenko, K. C. Prince, M. Coreno, A. Amore Bonapasta, L. Avaldi, *J. Phys.Chem. A*., 2009, **113***,*13593.
48 F. Rondino, D. Catone, G. Mattioli, A. Amore Bonapasta, P. Bolognesi, A. R. Casavola, M. Coreno, P. O'Keeffe, L. Avaldi*RSC Adv*. 2014, **4***,*5272.
49 A.Hagfeldt, G. Boschloo, L. Sun, L. Kloo, H.Pettersson,*Chem. Rev*. 2010, **110**, 6595.
50 K. Hara, Y. Dan-oh, C. Kasada, Y. Ohga, A. Shinpo, S. Suga, K. Sayama, H. Arakawa, *Langmuir* 2004, **20**, 4205.
51 A. Kay, M. Grätzel,*J. Phys. Chem.* 1993, **97**, 6272.

A novel green benzoporphyrin has been synthesized, characterized, studied by theoretical methods and tested in DSSC devices. Ab initio simulations predict the actual charge displacement during $S_0 \rightarrow S_1$ excitation.

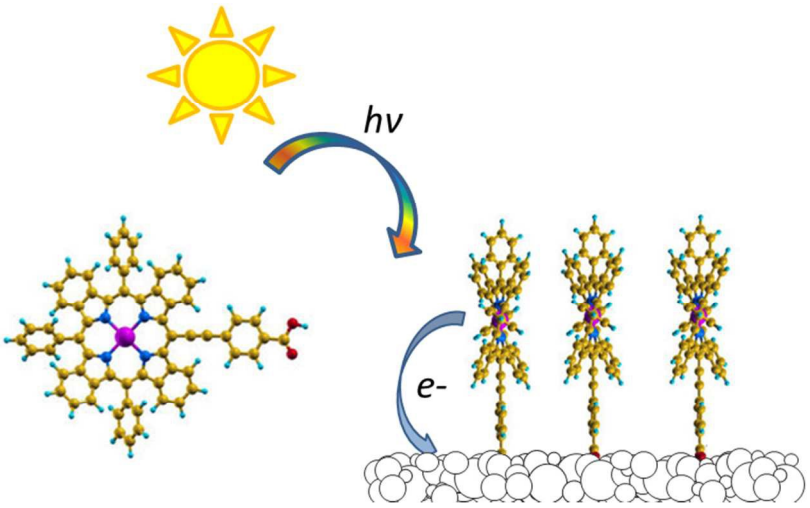

80x39mm (300 x 300 DPI)